# Dual-3D Femtosecond Laser Nanofabrication Enables Dynamic Actuation

Yong-Lai Zhang,*,[†] Ye Tian,[†] Huan Wang,[†] Zhuo-Chen Ma,[†] Dong-Dong Han,[†] Li-Gang Niu,[†] Qi-Dai Chen,[†] and Hong-Bo Sun*,[†,‡]

[†]State Key Laboratory of Integrated Optoelectronics, College of Electronic Science and Engineering, Jilin University, Changchun 130012, China

[‡]State Key Laboratory of Precision Measurement Technology & Instruments, Department of Precision Instrument, Tsinghua University, Haidian District, Beijing 100084, China

Ⓢ Supporting Information

**ABSTRACT:** Strategies that can make general materials smart are highly desired for developing artificial shape-morphing systems and devices. However, at present, it still lacks universal technologies that enable designable prototyping of deformable 3D micro-nanostructures. Inspired by natural automation systems, for instance, tendrils, leaves, and flowers deform dynamically under external stimuli by varying internal turgor, we report a dual-3D femtosecond laser processing strategy for fabricating smart and deformable 3D microactuators based on general photopolymers. By programming the size and distributions of voxels at the nanoscale, both the 3D profile and the 3D internetwork of a general photopolymer could be tailored in a controlled manner; thus, 3D microstructures encoded with precisely tailored networks could perform predictable deformations under certain stimuli. Using this dual-3D fabrication approach, energetic 3D microactuators, including a smart microflower, a responsive microvale, and an eight-finger microclaw, that permit controllable manipulation have been successfully developed.

**KEYWORDS:** 3D fabrication, femtosecond laser, smart materials, actuators, solvent responsive

S mart materials that can convert environmental stimuli into mechanical actions are very promising for developing automation systems, such as smart micro-robots and bio-MEMS,[1−7] because controllable manipulation can be readily realized without coupled energy supply systems or complex instruments. In past decades, typical smart materials, including both intrinsic stimuli-responsive materials (SRMs) with inherent responsive properties[8,9] and structured SRMs based on multilayer structures,[10,11] have been widely used for controllable actuation and have revealed great potential for smart devices. Generally, intrinsic SRMs deform under external stimuli due to the rearrangement of chemical bonds or molecular structures;[12,13] for instance, the photo-isomerization of azobenzene and its related materials leads directly to mechanical motions.[14] Multilayer SRMs, for instance, bimetallic strips, are deformable due to the strain mismatch among different layers.[15] The designable processing of such smart materials makes it possible to fabricate smart actuators that can perform desired tasks under a variety of stimuli.[16] In particular, when the dimension of the afore-mentioned smart materials is reduced to microscale, the interface properties may become dominant. Actuators at

microscale would be very sensitive to external stimuli, thus their actuating performance, such as response/recovery time and deformation degree, can be promoted significantly. However, both intrinsic SRMs and multilayer SRMs suffer from severe problems in the fabrication and integration of actuators at microscale. Generally, intrinsic SRMs suitable for classical microfabrication technologies are not commercially available. Considerable difficulties arise in the synthesis, processing, and integration of such materials, hindering their applications in microactuators. Furthermore, the response of a single SRM is usually governed by molecular structures, making them incapable of performing complex and desired deformations.[17] As an appealing alternative, multilayer SRMs that can be readily prepared by multimaterial deposition have been widely employed for developing actuators. In particular, by patterning the multilayer materials into different geometries, complex and predicable deformations, such as bending, folding, curling, and twisting, can be achieved based on a
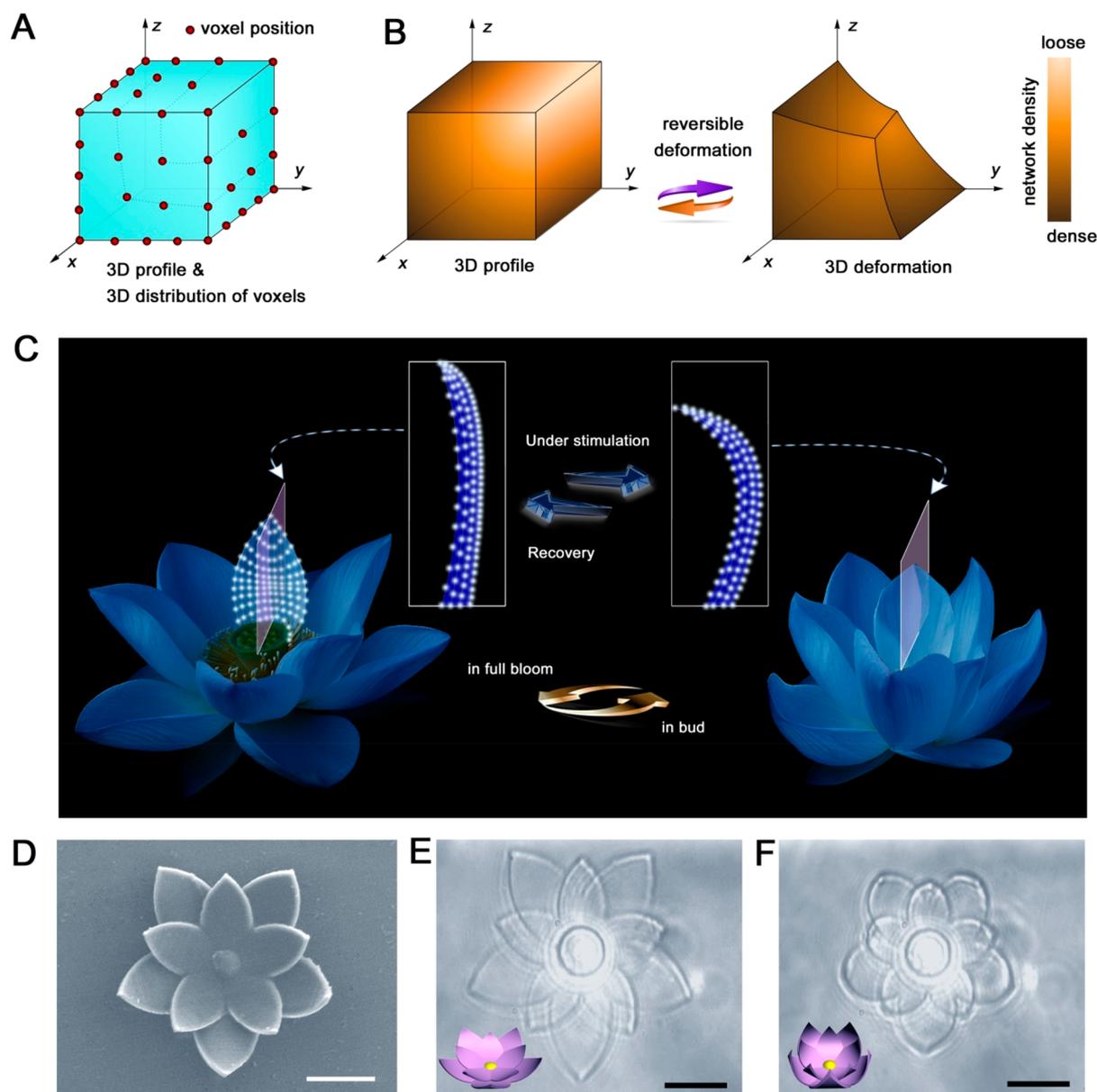
Figure 1. Basic design principle of dual-3D femtosecond laser fabrication. (A) Schematic illustration of 3D tailoring of the voxel distribution within a 3D model (dual-3D fabrication). (B) 3D microstructure fabricated by dual-3D fabrication permits reversible and predictable deformation under stimulation. (C−F) Design and fabrication of a smart microflower by dual-3D femtosecond laser processing. The network of each petal of the microflower has been programmed by tuning laser scanning SL, in which the SL gradually increased from 100 nm (outside layer) to 350 nm (inside layer). Under certain stimuli, the smart microflower can be manipulated between "bloom" and "bud" morphologies. (D) SEM image of the smart microflower. (E,F) Optical microscopic images of the microflower immersed in acetone (E) and n-hexane (F). The insets are 3D models of the bloom and bud shapes of the microflower. The scale bar is 10 $\mu$m.

wide range of materials.[18−20] However, problems with respect to the interlayer adhesion always threaten the stability of this kind of actuators because the deformation is derived from strain mismatches among different layers. To overcome this drawback, Gracias et al. successfully demonstrated the self-folding polymers with cross-link gradients. Instead of using bilayer structures, they reported the differentially photo-cross-linked SU-8 films for smart actuation and self-assembling microfluidics.[21] Subsequently, the same groups fabricated stimuli-responsive microscale actuators based on hydrogel using a photolithographic approach. Self-folding devices that consist of thin, gradient cross-linked hinges and thick, fully cross-linked panel have been successfully developed.[22] Yang et

al. reported a thin film buckling system based on SU-8 by creating a depth-wise gradient modulus after photo-cross-linking.[23] Although the aforementioned actuators can deform into 3D structures based on the cross-link gradients, they are essentially 2D devices. These inherent drawbacks significantly limit their applications in 3D microrobots. Thus, controlling the polymer cross-link gradient within 3D structures is highly desired, but it remains a big challenge. To realize 3D actuators, advanced fabrication technologies including femtosecond laser direct writing (fsLDW) and 3D printing have been employed to make deformable structures or devices. As typical examples, Gladman et al. reported the biomimetic 4D printing of composite hydrogel containing cellulose fibrils for controllable
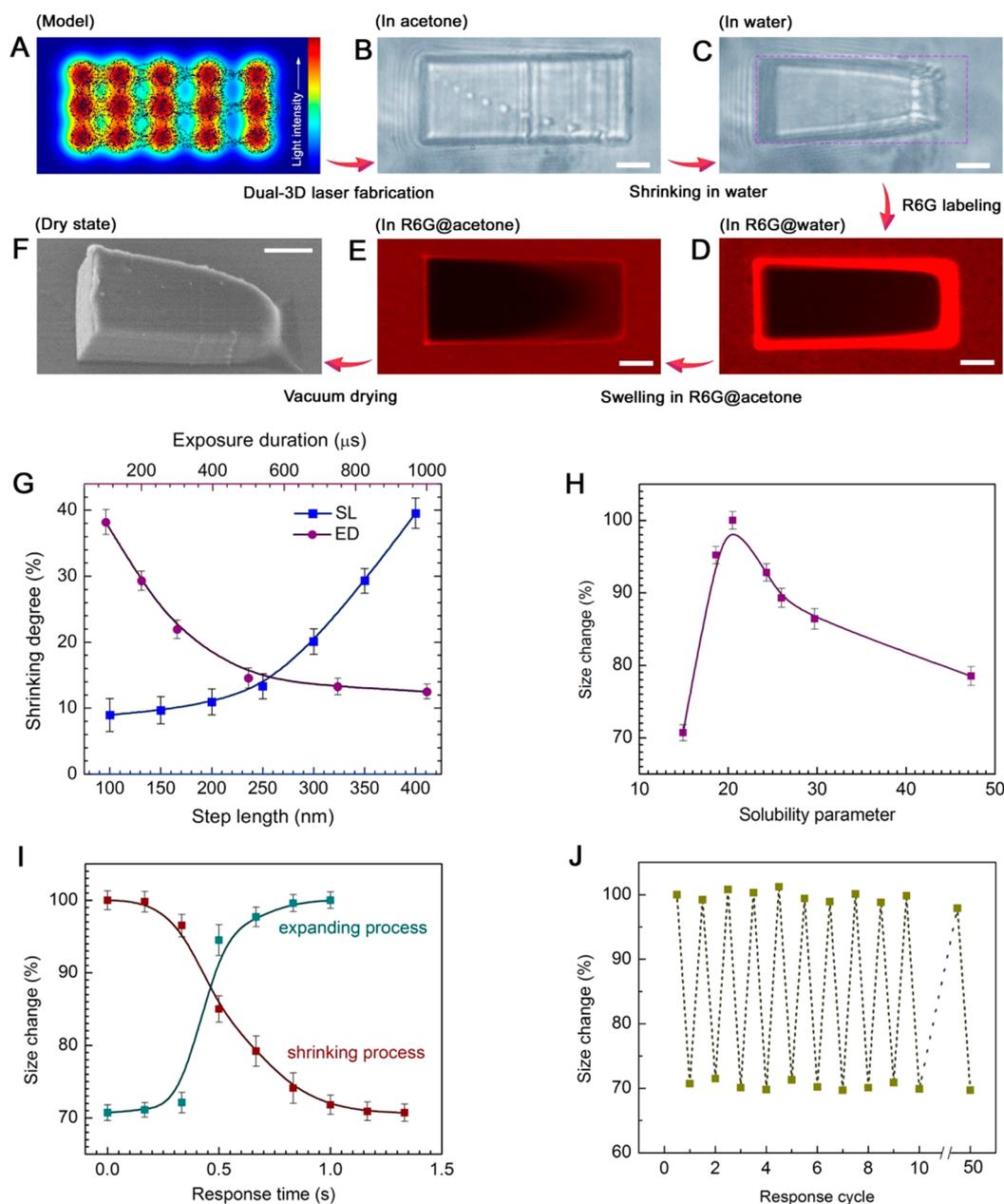
Figure 2. Dual-3D fabrication of a simple nonuniform block model and its responsive properties. (A) Light intensity distribution of 3 × 5 voxels with different SL values (the resultant polymer network is schematically illustrated). (B,C) Optical microscopic images of the smart block immersed in acetone and water, respectively. (D,E) Confocal fluorescence microscopic images of the smart block immersed in RhB@ water and RhB@acetone, respectively. (F) SEM image of the block in vacuum. The scale bar is 10 μm. (G−J) Responsive properties: (G) dependence of the response degree (shrinkage degree) on the laser scanning SL and ED; (H) dependence of the response degree on the SPs of different solvents; (I) dependence of the response degree (size change) on the responsive times for both shrinkage and recovery (expansion) processes; (J) size changes in both shrinkage and recovery (expansion) processes over 50 cycles.

actuation of ministructures.[24] Martella *et al.* fabricated a light-sensitive microhand by direct laser writing based on a custom-made liquid-crystal network.[25] Currently, despite the fact that smart actuation has been realized by processing deformable materials or introducing property gradient in special materials, universal processing technologies that permit the designable prototyping of arbitrary 3D microstructures, and at the same time enable making these microstructures smart, are still lacking.

As a powerful 3D processing technology, fsLDW has already proved its value in 3D micro-nanofabrication and has shown many advantages, such as high spatial resolution, high

accuracy, and programmable fabrication that cannot be achieved with other technologies.[26−31] Inspired by natural deformable systems, such as tendrils, leaves, and flowers that can deform dynamically under external stimuli by varying internal turgor, we reported here the fsLDW fabrication of smart microactuators by programming the 3D networks of general acrylate-based photopolymers at nanoscale. Essentially, in addition to the construction of a 3D profile, fsLDW also permits exquisite control over the size and 3D distribution of voxels by programming the laser processing parameters, such as the laser scanning path, step length (SL), and exposure duration (ED) of each voxel,[32,33] providing the possibility of

continuously tailoring polymer networks at the nanoscale. By controlling both the 3D profile and the 3D internetwork (dual-3D), 3D smart microactuators that can perform predictable deformations under certain stimuli have been readily fabricated.

## RESULTS AND DISCUSSION

Figure 1A shows a schematic illustration of the basic design principle for the dual-3D laser processing. It is well-known that any complex 3D microstructure can be readily fabricated by scanning a tightly focused laser beam according to a predesigned 3D model as the photopolymerization only occurs at the focal point due to the nonlinear absorption, mainly two-photon absorption. However, in most cases, uniform scanning of the laser focal spots is used to obtain a homogeneous polymer network. In our work, during the laser scanning of the 3D profile, we further tailored the polymer networks at the nanoscale by programming the 3D distributions and sizes of the voxels. The voxel distribution can be programmed by setting a variable laser scanning path and SL, whereas the voxel size can be controlled by tuning the ED of each voxel (Figure S1). Therefore, neo-concept dual-3D laser processing technology is proposed because the resultant 3D microstructures are stimuli-responsive and can deform in a predictable manner (Figure 1B).

To validate this idea experimentally, we designed and fabricated a smart microflower (Figure 1C−F) consisting of 10 petals and one flower core anchored to the substrate. Each petal comprises four layers in which the laser scanning SL gradually increases from 100 nm (outside) to 350 nm (inside). According to this model, a smart microflower with the total feature size of ~30 μm was fabricated (Figure 1C). Interestingly, when the microflower was immerged in acetone, the flower was in full bloom, whereas when the media solvent was changed to n-hexane, the petals of the flower curled, and the flower resembled a bud coming into bloom. Notably, this blooming is reversible, and the in-bud morphology could be easily switched (video S1).

To obtain an in-depth understanding of the responsive mechanism, we fabricated a simple anisotropic block by varying the laser scanning SL. The SL along the horizontal direction (x-axis) was gradually changed from 50 to 450 nm with a 2 nm increment, whereas the scanning SL along the vertical (y-axis) and altitudinal (z-axis) directions was fixed at 200 nm. Thus, asymmetric scanning was performed to fabricate a predefined microstructure. For two-photon photopolymerization, reactions occur only at the site where the photon density is high enough, and complicated 3D microstructures can be built from the voxels that overlap with each other. By tailoring the voxel distribution, a microblock with a gradually changed polymer network along the horizontal direction can be fabricated, as schematically illustrated in Figure 2A. As the unpolymerized monomers or molecular segments could be removed during the developing process, a much looser polymer network formed in the region on the right where the SL was larger.

The fsLDW fabrication allows the prototyping of 3D microstructures exactly according to the computer-designed patterns. The as-obtained block structure shows an almost perfect rectangular morphology without any distortion after developing in acetone (Figure 2B). However, when the solvent was replaced by water (pH 7), the right of the oblong block shrank significantly, whereas the left shows only slight shrinking, forming a trapezium shape (Figure 2C). This asymmetrical morphology change could be reversibly controlled by switching the surrounding solvent between acetone and water (Supporting Information, video S2). This interesting response property is well explained by the Hildebrand solubility parameter (SP) principle.[34] The Hildebrand solubility parameter (δ) provides a numerical estimate of the degree of interaction between solids and solvents and can be a good indication of solubility for many polymers. Materials with similar solubility parameters will be able to interact with each other, resulting in solvation, miscibility, or swelling. The SP of solidified PBMA was established to be ~19.1 MPa$^{1/2}$, and the solvents with SP differences smaller than 2 MPa$^{1/2}$ could be considered good solvents for PBMA. Because acetone has a very similar SP value of 19.7 MPa$^{1/2}$, the photopolymer oblong block would swell in it and support the whole structure. According to the reported results, acrylate-based polymers show very slow and unobvious swelling effect in poor solvents, such as water.[35] When the block was immersed in water, which has a much larger SP of 48.0 MPa$^{1/2}$, obvious shrinkage was observed in the region on the right where the polymer networks are very loose. Based on the microscopic images, the volume change was estimated to be ~35% compared with the swelling one, assuming the height of the structure keeps a constant value. The mechanism for the swelling/shrinking-induced response property was further confirmed by confocal fluorescence microscopic images, as shown in Figure 2D,E. In this test, water and acetone solvents labeled by rhodamine B (RhB) were used to stimulate the anisotropic block. When the block was immersed in RhB@water, the surrounding solvent was red due to the presence of RhB, whereas the shrunk block (trapezium) was dark, indicating the absence of RhB. In contrast, when the surrounding environment was replaced by the RhB@acetone solution, the trapezium structure recovered its rectangular morphology. Additionally, a gradually deepened red color (from left to right) appeared, indicating the swelling of the structure in acetone. The scanning electron microscopy (SEM) image captured in vacuum also confirmed the anisotropy in the network density of the block (Figure 2F), revealing that the right side of the block was nearly collapsed due to the very loose polymer network. Even though swelling is a very common phenomenon in polymers, programmable control of the 3D network density of general photopolymers at the nanoscale has not yet been reported. In this work, neo-concept dual-3D femtosecond laser fabrication was successfully proposed. This technique provides an opportunity to directly manipulate the swelling or shrinking behaviors of any polymeric microstructures in a controlled manner.

To tailor the polymer network precisely, both the voxel distribution and voxel size must be taken into account. We changed the SL and ED of each voxel to tune the response properties. As shown in Figure 2G, we first fixed the ED at 200 μs. As the SL increased from 100 to 400 nm, the degree of shrinkage increased from ~9 to ~40% after the solvents were switched from acetone to n-hexane. In particular, when the SL exceeded 250 nm, significant shrinkage was observed, indicating that laser scanning SL values larger than 250 nm would lead to a loose polymeric network and notable shrinkage in poor solvents. However, the modulation of the SL is not unlimited, and a further increase in the SL (beyond 400 nm) would result in a discontinuous structure. As the size of a single voxel is determined by ED (Supporting Information Figure S1), we also evaluated the effect of the ED on the response. In
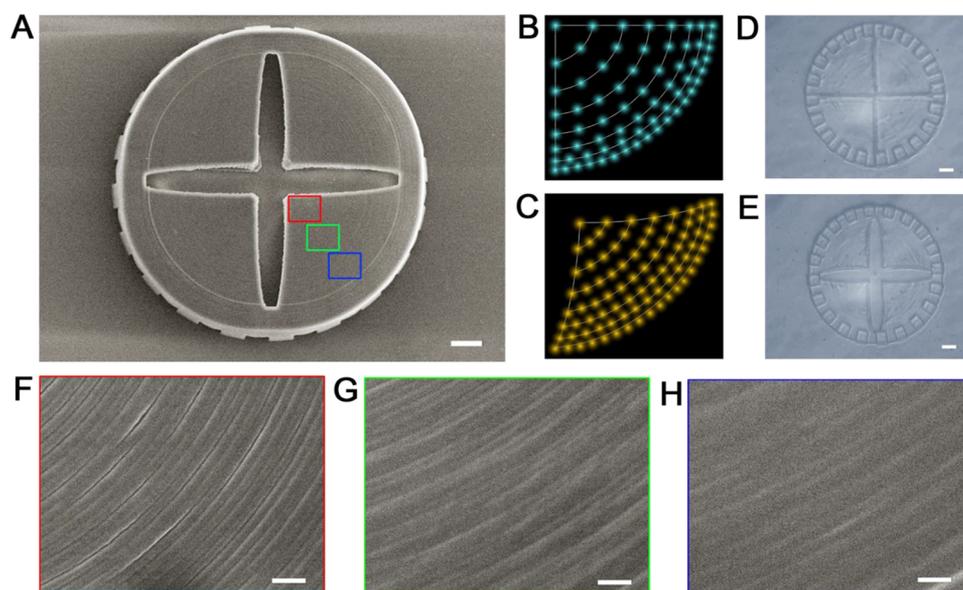
**Figure 3.** Design and fabrication of smart microvalve by dual-3D femtosecond laser fabrication. (A) SEM image of a smart microvalve with four fan shapes. (B) Schematic illustration of the laser spot scanning map of one sector. (C) Schematic illustration of the reconfiguration of the sector network. (D,E) Optical microscopic images of the smart microvalve immersed in acetone and *n*-hexane, respectively. For (A,D,E), the scale bars are 10 $\mu$m; (F−H) SEM images of different regions marked in (A). Scale bars are 1 $\mu$m.

this case, we fixed the SL at 350 nm and changed the ED from 100 to 1000 $\mu$s. As shown in Figure 2G, as the ED of a single laser spot increased, the response decreased from ~38 to ~12%. Generally, a long ED increases the voxel size, leading to relatively dense polymer networks, whereas a short ED results in a relatively smaller voxel size and, thus, loose polymer networks.

As mentioned previously, the response properties of a loose photopolymer network are determined by the SPs of the solvents. In our work, the dependence of the size change on seven typical solvents with different SPs in the range of 14.9−48.0 MPa$^{1/2}$ were investigated quantitatively (Figure 2H). Taking the structure fabricated with an SL of 350 nm and ED of 200 $\mu$s as a representative example, as the SP increased, the maximum value of the polymer size was observed at ~20 MPa$^{1/2}$ when acetone was used as the solvent. Immersing the photopolymer structures in other solvents with increased or decreased SP would lead to significant shrinkage. We note that the SP of *n*-hexane is only ~14.9 MPa$^{1/2}$, and that the deformation degree (30% of shrinkage) was observed when *n*-hexane was used as the solvent.

In addition to the magnitude of the response, another important factor is the response time. In this work, both the expansion process in acetone and the shrinkage process in *n*-hexane of a typical structure (350 nm for SL, 200 $\mu$s for ED) were investigated. In the shrinkage process, the volume change from 100 to ~70% takes only approximately 1 s, indicating a rapid response, whereas in the recovery process, the expansion requires just ~0.4 s (Figure 2I). The rapid response can be attributed to the microscale structures, for which the surface to volume ratio is much larger than that of bulk polymers. Thus, the mass transfer in microscale structures is relatively fast, and the response time for swelling and shrinking is short. Because of their sensitive shrinkage and recovery, these materials may hold great promise for potential use as sensitive micro-actuators. The reversible switching between shrinkage and expansion was also tested to evaluate the reproducibility and

stability (Figure 2J). Even after 50 instances of reversible switching, the magnitude of the structural changes remained almost constant.

Femtosecond laser dual-3D processing permits the flexible design and fabrication of various smart microstructures. The first example is a smart microvalve (Figure 3A). Here, a round valve, which had a diameter of ~90 $\mu$m, was divided equally into four fans. In each sector, the laser scanning SL was gradually tuned from 300 nm (outer loop) to 100 nm (inner loop). Figure 3B schematically shows the distribution of the laser spots. This figure quite clearly demonstrates that, in the center of the sector, the polymer network is very loose, whereas in the outer region, the network is much denser. Consequently, under the stimulation of poor solvents, such as *n*-hexane, the sector would shrink, as shown in Figure 3C. Optical microscopic images of the smart microvalve immersed in acetone and *n*-hexane show its "open" and "closed" states (Figure 3D,E and supporting video S3). Additionally, magnified SEM images directly confirm the presence of anisotropic polymer networks, and the laser scanning path can be clearly observed in the central region (Figure 3F). As the laser scanning SL decreased from the inner region to the outer region, the overlapping of laser scanning loops become unclear, indicating the presence of a smooth surface and dense networks (Figure 3G,H). By integrating such smart micro-valves with microfluidic devices, the fluid flow rate could be self-controlled according to the SPs of the solvents.

A microclaw array with eight smart fingers and an octagonal base attached to the substrate were also demonstrated (Figure 4A). The responsive fingers were fabricated by scanning four layers using different laser scanning SL values. The laser scanning SL gradually increased from 100 nm (outer layer) to 350 nm (inner layer), and a detailed model is shown in Figure S2. The SEM image shows that the size of a single microclaw is approximately 30 $\mu$m and that each microfinger is ~3 $\mu$m wide (Figure 4B). The microclaw could be controlled to perform snatching and releasing actions in a reversible manner, similar
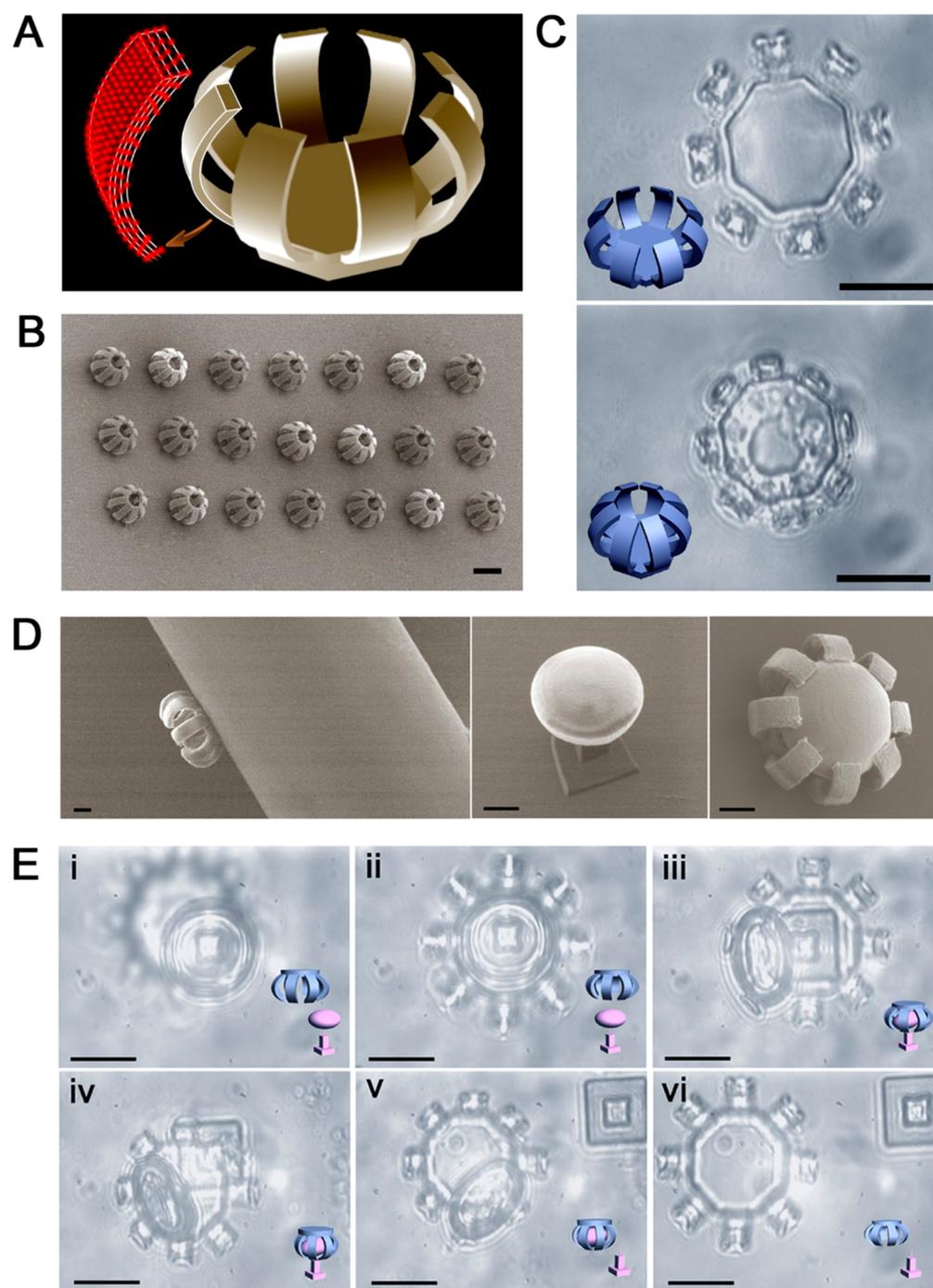
Figure 4. Design and fabrication of a smart microclaw. (A) Designed 3D max model of a smart microclaw. (B) SEM image of the resultant microclaw arrays. (C) Optical microscopic images of a microclaw in acetone (top) and *n*-hexane (bottom). The insets are 3D models. The scale bars are 20 *μ*m. (D) SEM images of the microclaw integrated with a microfiber mounted on a 3D-moving platform, the target microsphere anchored to a pedestal, and the microclaw with captured microsphere (from left to right). The scale bar is 10 *μ*m. (E) Process of picking up and releasing of the target microsphere by manipulating the microclaw: (i) microclaw over the microsphere (the inset is the side view of the target microsphere); (ii) collimation of the micromanipulator with the microsphere; (iii) contacting with the microsphere; (iv) catching hold of the microsphere after solvent switching (from acetone to *n*-hexane); (v) picking up the microsphere from the square pedestal; (vi) releasing the microsphere after solvent switching (from *n*-hexane to acetone). The scale bars are 20 *μ*m.

to the muscle of Mollusca (Figure 4C and supporting video S4).

Dual-3D femtosecond laser fabrication is not limited to planar substrates. In fact, it permits the integration of smart microactuators in any desired location. To manipulate the smart microclaw in a large space, we integrated it with a quartz microfiber mounted on a 3D movable platform (Figure 4D, left

image). Figure S2 shows the schematic illustration of the experimental setup. Using this approach, we could manipulate the microclaw freely to realize the desired performance. As a target object, a microsphere anchored to a pedestal was fabricated (Figure 4D); the entire process of the picking up and releasing the target microsphere is shown in Figure 4E. After collimation of the microclaw with the microsphere, the

microclaw clutches the microsphere when the solvent is switched to *n*-hexane and picks it up from the pedestal when the microfiber is moved. Finally, when the solvent is switched to acetone again, the microsphere is released. As the manipulation of such a microclaw does not require any external energy supply, and the performance is controllable and reversible, such smart actuators may find broad applications in multifunctional lab-on-a-chip systems. Additionally, with the rapid progress of microfluidics, the switching of solvents will become more convenient. In this regard, the integration of such smart actuators would enable complex on-chip operations and will make future microfluidic chips more intelligent.

## CONCLUSION

We have demonstrated the fsLDW-enabled 3D programming of photopolymer internetworks for designable fabrication and flexible integration of 3D microactuators. Controllably programming the voxel size and distribution by varying SL and ED makes it possible to spatially tune the network density of a solo photopolymer at the nanoscale, which imparts sensitive stimuli-responsive properties to these structures and enables reversible actuation using different solvents. Based on this basic design principle, smart microrobots that could be controllably manipulated to perform predictable deformation have been readily fabricated. More importantly, the direct laser writing processing also permits flexible integration of various microactuators with given devices, revealing the potential of developing complex sensing and actuating systems. We believe that, in the near future, the femtosecond laser smart processing technology could be widely employed to make smart materials with 3D features, contributing to the development of 3D microrobots.

## EXPERIMENTAL SECTION

**Preparation of Photopolymers.** In a typical procedure, 0.1 g of 2,4,6-trimethylbenzoyldiphenylphosphine oxide and 0.1 g of phenylbis(2,4,6-trimethylbenzoyl)phosphine oxide were added into 0.9 g of butyl methacrylate (BMA, monomer). After ultrasonic treatment for 20 min, 1.4 g of propoxylated trimethylolpropane triacrylate (PO3-TMPTA, cross-linker) was dropped into the mixture. After that, the mixture was ultrasonically vibrated for another 30 min, and the methacrylate-based photopolymer is finally achieved. The resultant photopolymer was protected in darkness for use.

**Fabrication of the Microstructures.** A typical setup for TPA fabrication consists of four parts: a laser source and light-direction system, a beam-focusing and motion-stage system, a computer-aided control system, as well as a charge-coupled device-based monitoring system. Motion-stage systems are usually high-precision piezoelectric stages combined with galvano-mirror scanners and linear stages (for large range fabrication). Piezo stages possess ~1 nm positioning precision, but their speed is limited to a maximum of 100 $\mu$m/s, and working field is also restricted to typically <500 $\mu$m. A mirror scanning system using galvanometric scanners is quite suitable for making microstructures with intricate geometry faster, as it virtually has no mechanical inertia, but the structure size is restricted by the objective field of view.

In this work, femtosecond laser pulses with central wavelength of 790 nm, pulse width of 120 fs, and repetition rate of 80 MHz were used for the fabrication. The laser was focused into the photopolymers by a 60× oil immersion objective lens with a high numerical aperture (NA = 1.35). The laser focal spot was scanned point by point according to the preprogrammed patterns; it was precisely controlled by a galvano-mirror pair in the lateral dimensions and a piezo stage in the lengthwise dimension. The laser power of polymerization was 6 mW, and the exposure duration at each dot and scanning step length were rationally designed according to different models. After scanning

the laser spot throughout the entire structure, the unpolymerized resin was removed in ethanol, and the final microstructure was obtained. For the fabrication of the "brick", the exposure duration was fixed at 200 $\mu$s; the step length was fixed at 200 nm along the *y*- and *z*-axes; the SL was gradually changed from 50 to 450 nm with an incremental change of 2 nm along the *x*-axis. For the fabrication of the microflower and the microclaw, the exposure duration was fixed at 200 $\mu$s; the step length was 200, 300, 400, and 500 nm from the outside layer to the inside layer. Detailed structures of the two models are presented in the Supporting Information (Figure S3).

**Manipulation of the Microactuators.** The manipulation of the microactuators was realized by switching the surrounding solvents. To manipulate the actuators in a large space, the smart microclaw can be integrated with a quartz microfiber that is mounted on a 3D movable platform, as shown in Figure S2. The 3D movement of the smart claw can be controlled by the movable platform. In this way, the collimation of the micromanipulator with the target, the picking up, and placing performance can be realized. The catching and releasing performance of the microclaw can be achieved by solvent switching.

**Characterization.** SEM images were measured on a JEOL JSM-6700F field-emission SEM operating at 3.0 keV. Optical micrographs were obtained from a Motic BA400 microscope. For confocal fluorescence microscope, the 488 nm lasers with the power density of 2.5 mW were used.

## ASSOCIATED CONTENT

### Ⓢ Supporting Information

The Supporting Information is available free of charge on the ACS Publications website at DOI: 10.1021/acsnano.8b08200.

> Light intensity distribution of a focal spot, achematic illustration of the experimental setup for microclaw manipulation, and models used for dual-3D fabrication (PDF)
>
> Solvent-responsive smart microflower (AVI)
>
> Solvent actuation of a photopolymer block with a network gradient (AVI)
>
> Solvent actuation of a smart microvalve (AVI)
>
> Solvent actuation of a smart microclaw (AVI)

## AUTHOR INFORMATION

### Corresponding Authors

*E-mail: yonglaizhang@jlu.edu.cn.
*E-mail: hbsun@jlu.edu.cn.

### ORCID Ⓓ

Yong-Lai Zhang: 0000-0002-4282-250X
Qi-Dai Chen: 0000-0002-0921-7973
Hong-Bo Sun: 0000-0003-2127-8610

### Notes

The authors declare no competing financial interest.

## REFERENCES

(1) Doring, A.; Birnbaum, W.; Kuckling, D. Responsive Hydrogels-Structurally and Dimensionally Optimized Smart Frameworks for Applications in Catalysis, Micro-System Technology and Material Science. *Chem. Soc. Rev.* **2013**, *42*, 7391−7420.

(2) Verma, R.; Adhikary, R. R.; Banerjee, R. Smart Material Platforms for Miniaturized Devices: Implications in Disease Models and Diagnostics. *Lab Chip* **2016**, *16*, 1978−1992.

(3) Jochum, F. D.; Theato, P. Temperature-and Light-Responsive Smart Polymer Materials. *Chem. Soc. Rev.* **2013**, *42*, 7468−7483.

(4) Liu, G. L.; Kim, J.; Lu, Y.; Lee, L. P. Optofluidic Control Using Photothermal Nanoparticles. *Nat. Mater.* **2006**, *5*, 27−32.

(5) Angelini, A.; Pirani, F.; Frascella, F.; Descrovi, E. Reconfigurable Elastomeric Graded-Index Optical Elements Controlled by Light. *Light: Sci. Appl.* **2018**, *7*, 9.

(6) Xu, B. R.; Tian, Z.; Wang, J.; Han, H.; Lee, T.; Mei, Y. F. Stimuli-Responsive and On-Chip Nanomembrane Micro-Rolls for Enhanced Macroscopic Visual Hydrogen Detection. *Sci. Adv.* **2018**, *4*, No. eaap8203.

(7) Xu, B. B.; Wang, L.; Ma, Z. C.; Zhang, R.; Chen, Q. D.; Lv, C.; Han, B.; Xiao, X. Z.; Zhang, X. L.; Zhang, Y. L.; Ueno, K.; Misawa, H.; Sun, H. B. Surface-Plasmon-Mediated Programmable Optical Nanofabrication of an Oriented Silver Nanoplate. *ACS Nano* **2014**, *8*, 6682−6692.

(8) Castet, F.; Rodriguez, V.; Pozzo, J. L.; Ducasse, L.; Plaquet, A.; Champagne, B. Design and Characterization of Molecular Nonlinear Optical Switches. *Acc. Chem. Res.* **2013**, *46*, 2656−2665.

(9) Sun, Y. L.; Dong, W.-F.; Yang, R. Z.; Meng, X.; Zhang, L.; Chen, Q.-D.; Sun, H.-B. Dynamically Tunable Protein Microlenses. *Angew. Chem., Int. Ed.* **2012**, *51*, 1558−1562.

(10) Han, D. D.; Zhang, Y. L.; Jiang, H. B.; Xia, H.; Feng, J.; Chen, Q. D.; Xu, H. L.; Sun, H. B. Moisture-Responsive Graphene Paper Prepared by Self-Controlled Photoreduction. *Adv. Mater.* **2015**, *27*, 332−338.

(11) Zhang, L.; Ruh, E.; Grutzmacher, D.; Dong, L. X.; Bell, D. J.; Nelson, B. J.; Schonenberger, C. Anomalous Coiling of SiGe/Si and SiGe/Si/Cr Helical Nanobelts. *Nano Lett.* **2006**, *6*, 1311−1317.

(12) Iamsaard, S.; Asshoff, S. J.; Matt, B.; Kudernac, T.; Cornelissen, J.; Fletcher, S. P.; Katsonis, N. Conversion of Light into Macroscopic Helical Motion. *Nat. Chem.* **2014**, *6*, 229−235.

(13) Huang, Y. G.; Shiota, Y.; Su, S. Q.; Wu, S. Q.; Yao, Z. S.; Li, G. L.; Kanegawa, S.; Kang, S.; Kamachi, T.; Yoshizawa, K.; Ariga, K.; Sato, O. Thermally Induced Intra-Carboxyl Proton Shuttle in a Molecular Rack-and-Pinion Cascade Achieving Macroscopic Crystal Deformation. *Angew. Chem., Int. Ed.* **2016**, *55*, 14628−14632.

(14) Zhang, X. Y.; Hou, L. L.; Samori, P. Coupling Carbon Nanomaterials with Photochromic Molecules for the Generation of Optically Responsive Materials. *Nat. Commun.* **2016**, *7*, 11118.

(15) Sahoo, S. C.; Sinha, S. B.; Kiran, M.; Ramamurty, U.; Dericioglu, A. F.; Reddy, C. M.; Naumov, P. Kinematic and Mechanical Profile of the Self-Actuation of Thermosalient Crystal Twins of 1,2,4,5-Tetrabromobenzene: a Molecular Crystalline Analogue of a Bimetallic Strip. *J. Am. Chem. Soc.* **2013**, *135*, 13843−13850.

(16) Wang, T.; Li, M.; Zhang, H.; Sun, Y.; Dong, B. A Multi-Responsive Bidirectional Bending Actuator Based on Polypyrrole and Agar Nanocomposites. *J. Mater. Chem. C* **2018**, *6*, 6416−6422.

(17) Kaehr, B.; Shear, J. B. Multiphoton Fabrication of Chemically Responsive Protein Hydrogels for Microactuation. *Proc. Natl. Acad. Sci. U. S. A.* **2008**, *105*, 8850−8854.

(18) Na, J. H.; Evans, A. A.; Bae, J.; Chiappelli, M. C.; Santangelo, C. D.; Lang, R. J.; Hull, T. C.; Hayward, R. C. Programming Reversibly Self-Folding Origami with Micropatterned Photo-Crosslinkable Polymer Trilayers. *Adv. Mater.* **2015**, *27*, 79−85.

(19) Malachowski, K.; Jamal, M.; Jin, Q. R.; Polat, B.; Morris, C. J.; Gracias, D. H. Self-Folding Single Cell Grippers. *Nano Lett.* **2014**, *14*, 4164−4170.

(20) Han, D. D.; Zhang, Y. L.; Liu, Y.; Liu, Y. Q.; Jiang, H. B.; Han, B.; Fu, X. Y.; Ding, H.; Xu, H. L.; Sun, H. B. Bioinspired Graphene Actuators Prepared by Unilateral UV Irradiation of Graphene Oxide Papers. *Adv. Funct. Mater.* **2015**, *25*, 4548−4557.

(21) Jamal, M.; Zarafshar, A. M.; Gracias, D. H. Differentially Photo-Crosslinked Polymers Enable Self-Assembling Microfluidics. *Nat. Commun.* **2011**, *2*, 527.

(22) Yoon, C. K.; Xiao, R.; Park, J. H.; Cha, J.; Nguyen, T. D.; Gracias, D. H. Functional Stimuli Responsive Hydrogel Devices by Self-folding. *Smart Mater. Struct.* **2014**, *23*, 094008.

(23) Chen, C. M.; Reed, J. C.; Yang, S. Guided Wrinkling in Swollen, Pre-patterned Photoresist Thin Films with a Crosslinking Gradient. *Soft Matter* **2013**, *9*, 11007−11013.

(24) Sydney Gladman, A.; Matsumoto, E. A.; Nuzzo, R. G.; Mahadevan, L.; Lewis, J. A. Biomimetic 4D printing. *Nat. Mater.* **2016**, *15*, 413−418.

(25) Martella, D.; Nocentini, S.; Nuzhdin, D.; Parmeggiani, C.; Wiersma, D. S. Photonic Microhand with Autonomous Action. *Adv. Mater.* **2017**, *29*, 1704047.

(26) Kawata, S.; Sun, H. B.; Tanaka, T.; Takada, K. Finer Features for Functional Microdevices - Micromachines Can Be Created with Higher Resolution Using Two-Photon Absorption. *Nature* **2001**, *412*, 697−698.

(27) Zhang, Y. L.; Chen, Q. D.; Xia, H.; Sun, H. B. Designable 3D Nanofabrication by Femtosecond Laser Direct Writing. *Nano Today* **2010**, *5*, 435−448.

(28) Park, S. H.; Yang, D. Y.; Lee, K. S. Two-Photon Stereolithography for Realizing Ultraprecise Three-Dimensional Nano/Microdevices. *Laser Photonics Rev.* **2009**, *3*, 1−11.

(29) Juodkazis, S. Manufacturing 3D Printed Micro-Optics. *Nat. Photonics* **2016**, *10*, 499−501.

(30) Sugioka, K.; Cheng, Y. Femtosecond Laser Three-Dimensional Micro- and Nanofabrication. *Appl. Phys. Rev.* **2014**, *1*, 041303.

(31) Chen, T. H.; Fardel, R.; Arnold, C. B. Ultrafast Z-Scanning for High-Efficiency Laser Micro-Machining. *Light: Sci. Appl.* **2018**, *7*, 17181.

(32) Sun, H. B.; Takada, K.; Kim, M. S.; Lee, K. S.; Kawata, S. Scaling Laws of Voxels in Two-Photon Photopolymerization Nanofabrication. *Appl. Phys. Lett.* **2003**, *83*, 1104−1106.

(33) Sun, H. B.; Maeda, M.; Takada, K.; Chon, J. W. M.; Gu, M.; Kawata, S. Experimental Investigation of Single Voxels for Laser Nanofabrication *via* Two-Photon Photopolymerization. *Appl. Phys. Lett.* **2003**, *83*, 819−821.

(34) Burke, J. *Part 2: Hildebrand Solubility Parameter*; The American Institute for Conservation, 1984; pp 121−122.

(35) Gervinskas, G.; Day, D.; Juodkazis, S. High-Precision Interferometric Monitoring of Polymer Swelling Using A Simple Optofluidic Sensor. *Sens. Actuators, B* **2011**, *159*, 39−43.